

Active Feedback Stabilization of Toroidal External Modes in Tokamaks

Y. Q. Liu and A. Bondeson

Department of Electromagnetics, EURATOM-NFR/Fusion Association, Chalmers University of Technology,
S-412 96 Göteborg, Sweden
(Received 20 September 1999)

Active feedback stabilization of pressure-driven modes in tokamaks is investigated by toroidal computations. Typically, the feedback does not strongly modify the plasma-generated magnetic field perturbation. Feedback with modest gain and a single coil array poloidally stabilizes substantially for a range of coil shapes. Optimum design uses narrow sensor coils not too far from the plasma and rather wide feedback coils, which may be outside the resistive wall. Complex gain, which makes the mode rotate, can decrease the gain required for stabilization, but real gain is more robust.

PACS numbers: 52.55.Fa, 28.52.Av, 52.35.Py, 52.65.Kj

Advanced tokamaks, with improved confinement in a central region of weak or negative shear [1,2], offer prospects of achieving fusion in an economically competitive way. However, to achieve steady state operation with high beta, magnetohydrodynamic (MHD) modes of low toroidal mode number n need stabilization from a conducting wall, unless the cross section is very strongly shaped [3]. A resistive wall can stabilize over the resistive decay time of the wall, but stabilization on longer time scales requires additional techniques such as plasma rotation [4–9] or active feedback [10–14]. Unfortunately, the plasma rotation speeds required for stabilization are unattractively high [4,8,9]. By contrast, active feedback is used routinely to stabilize the $n = 0$ vertical instability [15]. This has permitted stronger shaping and has significantly extended tokamak performance. Experiments on feedback stabilization of $n \neq 0$ modes are currently in progress on the DIII-D tokamak [16].

Feedback of nonaxisymmetric modes is complex because of the mode structure, and a realistic numerical model is very useful for optimizing the system. While axisymmetric feedback is well understood [15], $n \neq 0$ feedback is, so far, treated mainly by cylindrical theory [10–13]. We have added sensor and feedback coils to the MARS stability code [4–6] and now have a toroidal MHD model for feedback stabilization. The first results are reported here.

We consider feedback and sensor coils, located on toroidal surfaces that are conformal, in poloidal planes (toroidal angle $\phi = \text{const}$), with the vacuum-plasma boundary (see Fig. 1). Also the resistive wall is conformal to the vacuum-plasma boundary and, e.g., $r_w = 1.2a$ means that the wall is 1.2 times larger linearly than the vacuum-plasma boundary. The feedback and sensor coils consist of segments oriented in the toroidal (ϕ) and poloidal (χ) directions. The number of coils in the toroidal direction is assumed large enough so that the feedback current can be described as a single n surface current $\text{Re}[\vec{J}_f(\chi) \exp(in\phi)]$. For the present study, we consider *one* set of feedback and sensor coils in the poloidal direction, both placed in the outboard midplane.

MARS uses Fourier expansion in χ , and it would require impractically many components to represent the angular dependence of thin-wire coils. Therefore, we have softened the angular dependencies by approximating a feedback conductor segment in the toroidal direction as a Gaussian (of width 0.3 radians in χ), centered at $\chi = \pm\alpha\pi/2$. We use equal arc coordinates; hence, α is the fraction of half the circumference, subtended by the active coil. We find that small sensor coils are optimal, because they maximize the ratio of flux from the plasma ($b_{np} = \hat{n} \cdot \vec{b}_p$ is approximately harmonic in χ around the midplane) to the flux from the feedback coil (b_{nf} has a local minimum in the midplane). This is favorable for stabilization. For the studies shown here, the sensor coils cover 2.5% of the poloidal circumference.

The current in the feedback coil is assumed proportional to the flux measured in the sensor coil. This reasonably models the present DIII-D experiments and gives a very simple description. The gain is defined as $G = -\psi_{sf}/\psi_{s,\text{tot}}$, where ψ_{sf} is the $\exp(in\phi)$ flux in the sensor coils produced by the feedback currents and $\psi_{s,\text{tot}}$ is the total $\exp(in\phi)$ flux in the sensor coils. For the total flux (TF) scheme, G is real and positive.

As a test case, we use the $n = 1$ instability of an “advanced” equilibrium with $q_{\text{min}} = 1.6$, $q_a \approx 3.4$, low

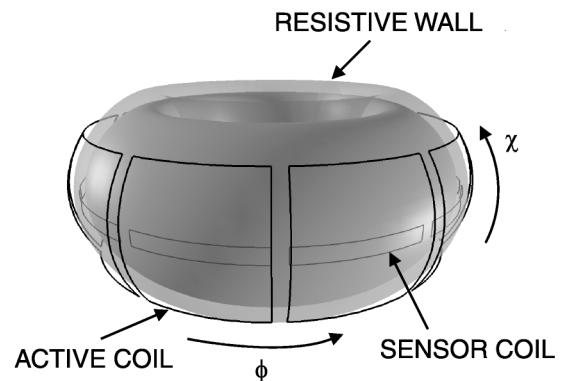


FIG. 1. Geometry of a tokamak with a feedback system for nonaxisymmetric modes.

inductance $l_i = 0.61$, normalized beta $\beta_N = \beta/(I/aB_0) \approx 4.7$, good bootstrap alignment, and moderate shaping: elongation 1.65 and triangularity 0.35. The pressure is far above the no-wall limit $\beta_N \approx 2.9$ and the marginal position of an ideal wall is $r_w = 1.3a$. The wall time is 20000 Alfvén times, and the growth rates are normalized with respect to the wall time.

Figure 2 shows the *critical gain*, i.e., the lowest $|G|$ that stabilizes the resistive wall mode, versus the poloidal width of the feedback coil for different phase angles of G , when the sensor is close to the plasma, $r_s = 1.05a$. For all the figures shown here, the resistive wall is placed at $r_w = 1.2a$, and the feedback coils are just outside the wall, $r_f = 1.225a$. The efficiency of the feedback depends on the coil width, and the minimum critical gain of about 1.2 occurs for $\alpha \approx 0.55$. Stabilization is possible for a rather wide range of coil widths, $0.38 \leq \alpha \leq 0.72$, so the feedback system should be reasonably robust to changes of the equilibrium. For an equilibrium with lower current ($q_{\min} = 2.5$), we find similar results as in Fig. 2, except the α values are smaller.

Concerning mode structures, the feedback typically does not change the plasma-generated magnetic field perturbation very much. As a measure of how the poloidal variation of different field components match one another, we use the correlation coefficient for the complex field amplitudes. [For two $n = 1$ amplitudes, this is defined as $C_{fg} = (f, g^*)/[((f, f^*)(g, g^*))^{1/2}]$ with $(f, g^*) = \int_{-\pi}^{\pi} f(\chi)g^*(\chi) d\chi$]. Figure 3 shows several correlation coefficients versus coil width. Surprisingly, the highest correlation of the normal flux from the feedback coil with the plasma-generated $b_{np}(\chi)$ (curve 1, at $\alpha \approx 0.4$) does *not* give optimum stabilization. Figure 3 indicates that a better design criterion is how well the feedback field matches the *normal derivative* of b_{np} (curve 2). We find that this holds also when there are three coils in the poloidal direction, and that the criterion involving $\partial b_n/\partial n$ gives better predictions than

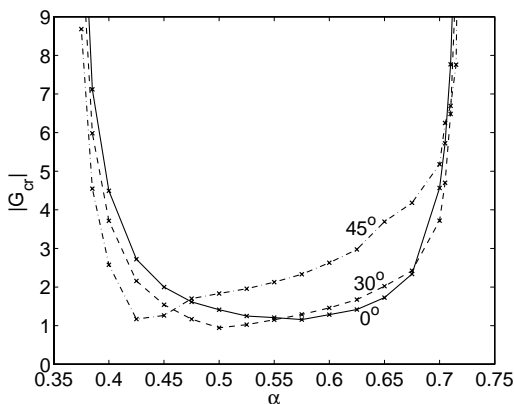


FIG. 2. Critical gain for stabilization versus poloidal extent of the feedback coils when $r_s = 1.05a$, $r_w = 1.2a$, and $r_f = 1.225a$ for different phase angles of the gain, indicated on the curves.

that of maximizing the overlap between the feedback and resistive wall currents. Note that at marginal stability for the TF scheme, the wall current vanishes. The feedback coil alone must then supply a field, which *together* with the plasma-generated vacuum field makes b_n and the perturbed total pressure $\vec{b} \cdot \vec{B} + p$ continuous at the plasma vacuum boundary. Neither of these sums vanishes, and it is *not* the job of the feedback coil to cancel the plasma contribution to either of them.

Often, low-order reduced models can accurately describe distributed systems. This works well for the vertical instability [15], and we find it very useful also for $n \neq 0$. Okabayashi *et al.* [13] derived a circuit model for a cylindrically symmetric feedback system, representing the plasma as a circuit having a self-inductance L_p^{eff} and a mutual inductance with the wall M_{pw} . An ideal wall stabilizes provided $\tilde{L}_w = L_w - M_{pw}^2/L_p^{\text{eff}} < 0$. In the absence of feedback, $\tilde{L}_w < 0$ implies that finite wall resistance R_w gives instability on the L_w/R_w time scale, the resistive wall mode. The TF feedback scheme can stabilize the resistive wall mode, provided that $\tilde{M}_{sf} = M_{sf} - M_{sp}M_{pf}/L_p^{\text{eff}} < 0$.

A similar lumped circuit model can be constructed for toroidal plasmas by applying a Galerkin method to Faraday's law, using several basis functions for the surface currents, e.g., on the wall $\hat{n} \times \Delta \vec{b} = \vec{J}_w = \sum_{i=1}^N I_{wi} \hat{n} \times \nabla u_i$ [14]. To show the consequences of a lumped circuit model, we consider N current patterns on the resistive wall, and ignore plasma inertia. The currents in the plasma I_{pj} , resistive wall I_{wj} , $J = 1, 2, \dots, N$, and feedback circuit I_f satisfy the following loop equations on the plasma surface, the resistive wall, and feedback circuit, respectively:

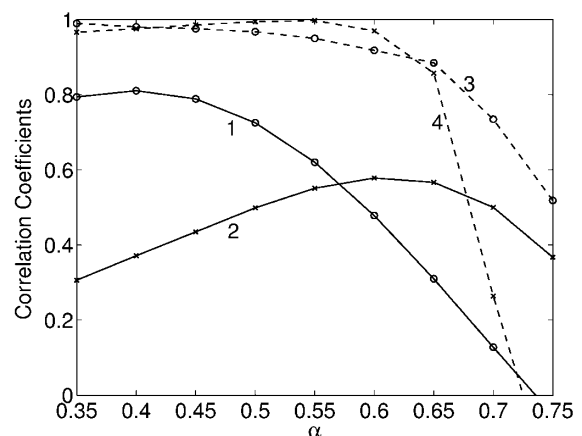


FIG. 3. Correlation coefficients (defined in the text) for poloidal variation of various field components versus feedback coil width. Correlation of the feedback field with the original mode; curve 1: $-b_n$, curve 2: $\partial b_n/\partial n$. Correlation of the plasma-generated perturbed field with and without feedback stabilization; curve 3: b_n ; curve 4: $\partial b_n/\partial n$. All the correlations are realvalued and were evaluated at the plasma vacuum boundary.

$$\sum_j M_{pi,pj}^{\text{eff}} I_{pj} + \sum_{j=1}^N M_{pi,wj} I_{wj} + M_{pi,f} I_f = 0, \quad i = 1, 2, \dots, \quad (1)$$

$$\sum_{j=1}^N (\gamma M_{wi,wj} + R_{wi,wj}) I_{wj} + \gamma \sum_j M_{wi,pj} I_{pj} + \gamma M_{wi,f} I_f = 0, \quad i = 1, 2, \dots, N, \quad (2)$$

$$M_{sf} I_f = -G \left(M_{sf} I_f + \sum_j M_{s,pj} I_{pj} + \sum_{j=1}^N M_{s,wj} I_{wj} \right). \quad (3)$$

Here γ is the growth rate, M denotes the various mutual inductances, and $R_{wi,wj}$ the joint resistance of two "circuits" (current basis functions) on the wall. The plasma currents can be eliminated from (2) and (3) by means of (1). This modifies the mutual inductances: $M_{wi,f} \rightarrow \tilde{M}_{wi,f}$, etc. in (2) and (3). Then, (2) can be used to express the wall currents in terms of the feedback current, $I_{wi} = I_f S_i(\gamma)/P(\gamma)$, where S_i and P are polynomials of degree N with $S_i(0) = 0$. Substituting this into (3), we have

$$G(\gamma) = \frac{-M_{sf} P(\gamma)}{\tilde{M}_{sf} P(\gamma) + \sum_{i=1}^N \tilde{M}_{s,wi} S_i(\gamma)} = \frac{P(\gamma)}{Q(\gamma)}. \quad (4)$$

P and Q are order N polynomials, and $G(0) = -M_{sf}/\tilde{M}_{sf}$ is independent of the resistive wall. Evidently, this model, ignoring plasma inertia and amplifier characteristics, includes time dependence only via the resistive decay of the wall currents, and the order of the system equals the number of current patterns on the wall, N . To have a reliable model valid for a wide range of conditions, N must be large (as it is in MARS). However, the MARS results show that when all parameters except G are specified, low-order models work very well.

Equation (4) suggests that $G(\gamma)$ computed with the full MARS model may be well fitted by a Padé approximation. For this purpose, we generalize slightly and allow P and Q to have different orders, M and N , and denote the corresponding Padé approximation as (M, N) . We run MARS to compute γ for different G and determine the coefficients of P and Q by imposing (4) for the computed cases. We then test the model by examining how well (4) predicts additional computed points. Generally, the (1, 1) model is poor, the (2, 2) approximation is acceptable at low frequency; however, the (3, 2) and (3, 3) approximations work over a much larger frequency range. Figure 4 shows $\gamma(G)$ for the same geometry as in Fig. 2 with $\alpha = 0.5$. The (3, 2) Padé approximation constructed from data for $\arg(G) = \pm 30^\circ$ agrees well with the full simulations for G real as well as $\arg(G) = 45^\circ$. [In this figure, the (3, 2) approximation cannot be distinguished from the (3, 3).] Using the

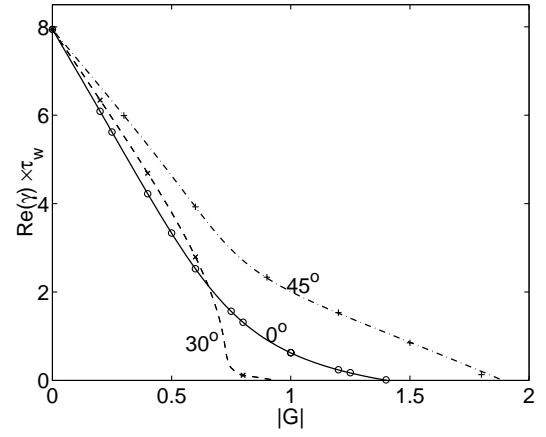


FIG. 4. Dependence of growth rate on gain for $\alpha = 0.5$. The points show full simulation results and the curves show the (3, 2) Padé approximation. Its coefficients were determined from three simulations with $\arg(G) = 30^\circ$.

(3, 2) Padé approximation, we get accurate predictions for all relevant G , from six runs of the full system. By using $\gamma(G^*) = \gamma^*(G)$, this can be reduced to three runs.

Stability boundaries for the complex gain occur at $G(i\omega)$, ω real. The low frequency part of such curves is shown in Fig. 5(a), for the (2, 2), (3, 2), and (3, 3) Padé approximations, together with some marginally stable G from MARS runs. The system is stable for G to the right of the contour. On the inner, circle like, low frequency part of the contours, where $|\omega \tau_w| \lesssim 2$, all approximations successfully represent the full simulation results. On the outer part, for higher frequencies, the differences are larger. Here, the (3, 2) and (3, 3) approximations are superior, and the (3, 2) is the best. The separation in frequency between the segments of the marginal stability contour is illustrated in Fig. 5(b), which shows the modulus and phase of G_{cr} as functions of the frequency. All approximations agree well for $|\omega \tau_w| \lesssim 2$, and the (3, 2) and (3, 3) are almost identical for $|\omega \tau_w| < 30$. Thus, the (3, 2) Padé approximation should be adequate over the bandwidth of practical feedback amplifiers. (We have assumed an idealized amplifier, but, if its circuit model is known, it can be incorporated in the analysis.)

Figure 5 indicates that the critical gain is reduced when G is complex, $\arg(G) \approx 30^\circ$. However, when one considers several cases, small phase angles give more robust behavior, and $\arg(G) \approx 20^\circ$ appears optimal. For larger phase angles, the limiting instabilities tend to occur at "high" frequency, $|\omega \tau_w| \gtrsim 5$. This is why G_{cr} is higher for phase angles of 30° and 45° for wide feedback coils in Fig. 2. For small α and $r_s \lesssim 1.1a$, the little loops to the left on the $G(i\omega)$ contour [which delimit regions with two unstable modes in Fig. 5(a)] shrink into cusps. The case in Fig. 5 cannot be stabilized with purely imaginary gain. In fact, we find no cases of complete stabilization with imaginary gain, the sensors inside, and the feedback coils outside the resistive wall.

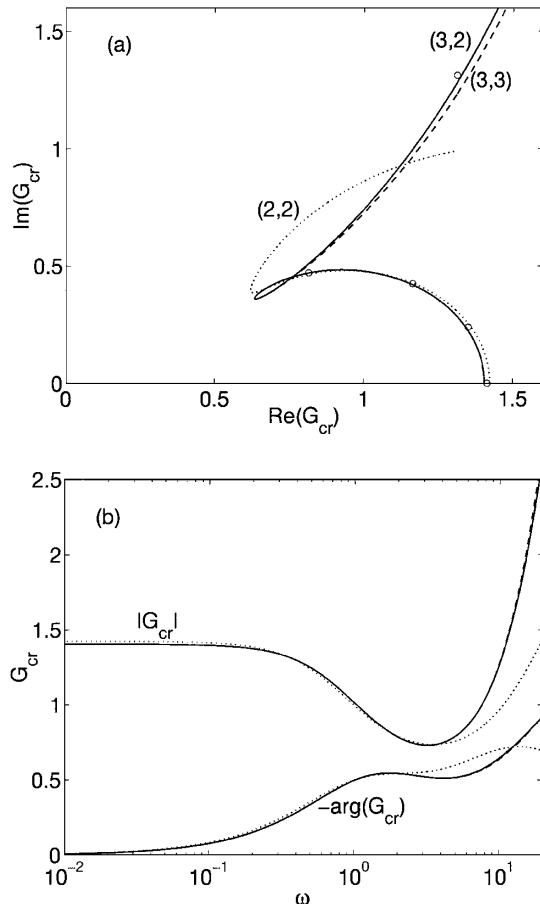


FIG. 5. Stability boundaries for complex gain and $\alpha = 0.55$, $r_s = 1.05a$. (a) $G(i\omega)$ for real ω from Padé approximations of different order. The stable region is to the right of the contours. (b) Modulus (upper curves) and phase (lower curves) of the critical G as functions of the frequency. Dotted curve: (2,2); solid curve: (3,2); dashed curve: (3,3) Padé approximations.

Figure 6 shows the critical gain versus the feedback coil width for different sensor coil radii. G_{cr} increases, and the useful range of feedback coil widths shrinks significantly, when the sensor coils are moved away from the plasma. The reason for this is that the ratio of plasma to feedback flux through the sensor coils decreases when r_s increases. It is difficult to stabilize our test equilibrium when the sensor coils are placed on the resistive wall. (There is a narrow stabilizable interval in α when $r_s = r_w = 1.2a$. However, the system is stable only in a small region in the complex G -plane, around a finite interval on the real G -axis.) In this connection, it should be pointed out that our present calculations use a wall radius relevant to present tokamaks, but, in reactors, the wall may be closer to the plasma, which could prohibit sensor coils inside the wall. The feedback system can be improved in several ways: by using more poloidal arrays, poloidal overlap, derivative gain, and sensors at several radii. We are examining the possibility of combining these techniques to find robust working scenarios with the sensor coils outside the wall. In contrast to the sensitive dependence on sensor location, the radius of the feedback coil has a rather weak influence.

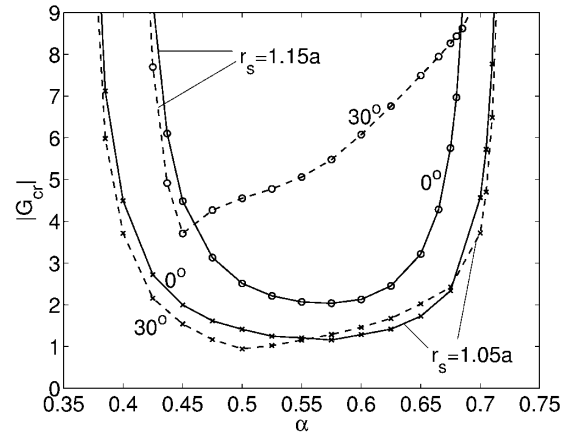


FIG. 6. Modulus of critical gain versus the feedback coil width for different sensor radii ($r_s = 1.05a$ and $r_s = 1.15a$) and differently phased feedback, $\arg(G) = 0, 30^\circ$.

In conclusion, strong instabilities can be stabilized with a single array of feedback coils outside the resistive wall. With an optimal design (narrow sensor coils not too far from the plasma and rather wide feedback coils), the critical gain is low. Thus, active feedback has the potential of raising the beta limit of advanced tokamaks. Here, we have considered only stabilization of one toroidal mode number $n = 1$. The stability of external modes with $n > 1$ also needs to be addressed.

We are grateful to Dr. Michio Okabayashi for generously sharing his knowledge of feedback stabilization.

-
- [1] C. Kessel *et al.*, Phys. Rev. Lett. **72**, 1212 (1994).
 - [2] E.A. Lazarus *et al.*, Phys. Rev. Lett. **77**, 2714 (1996).
 - [3] A. Bondeson *et al.*, Nucl. Fusion **37**, 1419 (1997).
 - [4] A. Bondeson and D.J. Ward, Phys. Rev. Lett. **72**, 2709 (1994).
 - [5] D.J. Ward and A. Bondeson, Phys. Plasmas **2**, 1570 (1995).
 - [6] M.S. Chu *et al.*, Phys. Plasmas **2**, 2236 (1995).
 - [7] R. Betti, Phys. Fluids **5**, 3615 (1998).
 - [8] A. Bondeson, C.G. Gimblett, and R.J. Hastie, Phys. Plasmas **6**, 637 (1999).
 - [9] A. Garofalo *et al.*, Phys. Rev. Lett. **82**, 3811 (1999).
 - [10] R. Fitzpatrick and T.H. Jensen, Phys. Plasmas **3**, 2641 (1996).
 - [11] R. Fitzpatrick, Phys. Plasmas **4**, 2519 (1997); **4**, 4043 (1997).
 - [12] R. Fitzpatrick and E.P. Yu, Phys. Plasmas **5**, 2340 (1998).
 - [13] M. Okabayashi, N. Pomphrey, and R.E. Hatcher, Nucl. Fusion **38**, 1607 (1998).
 - [14] A.H. Boozer, Phys. Plasmas **5**, 3350 (1998).
 - [15] E.A. Lazarus, J.B. Lister, and G.H. Neilson, Nucl. Fusion **30**, 111 (1990).
 - [16] M. Okabayashi *et al.*, in Proceedings of the 26th EPS Conference on Controlled Fusion and Plasma Physics, Paper No. P4.076, <http://epsppd.epfl.ch/>.